Orbital magnetism of graphene flakes

Yuya Ominato and Mikito Koshino

Department of Physics, Tohoku University, Sendai 980-8578, Japan

Orbital magnetism is studied for graphene flakes with various shapes and edge configurations using the tight-binding approximation. In the low-temperature regime where the thermal energy is much smaller than the energy-level spacing, the susceptibility rapidly changes between diamagnetism and paramagnetism as a function of Fermi energy, in accordance with the energy-level structure. The susceptibility at the charge neutral point is generally larger in armchair flake than in zigzag flake, and larger in hexagonal flake than in triangular flake. As the temperature increases, the discrete structures due to the quantum confinement are all gone, and the susceptibility approximates the bulk limit independently of the atomic configuration. The diamagnetic current circulates entirely on the graphene flake at zero temperature, while in increasing temperature it is localized near the edge with the characteristic depth proportional to $1/T$. We predict that the diamagnetism of graphene can be observed using the alignment of graphene flakes in a feasible range of magnetic field.

I. INTRODUCTION

The recent developments in fabrication of graphene-based systems realized a variety of graphene nanostructures, such as graphene ribbons[1–5] and graphene flakes.[6–10] The electronic band structure in these systems crucially depends on the shape and also on the edge termination,[6,11–13] giving physical properties distinct from those in bulk graphene. So far, a number of theoretical research has been devoted to understanding the electronic properties of graphene ribbons[11–18] and graphene flakes[19–26] with various atomic configurations.

The purpose of this paper is to study the orbital magnetism of graphene flakes. Experimentally, the magnetic property of graphene-based materials was investigated for bulk graphite,[27–29] nanographite,[30] and exfoliated graphene nanocrystals.[31] There the susceptibility always contains a strong diamagnetic background due to the orbital effect, whereas it is also contributed by the spin paramagnetism,[31] and in some cases the spontaneous spin magnetic ordering[28–30,32] which can be caused by the zero-energy edge states[13,33,34] and atomic defects. In any case, correct understanding of the orbital susceptibility of finite graphene systems is important to describe the overall magnetic property in realistic graphene systems.

Graphene has unusual electronic band structure characterized by the massless Dirac spectrum,[35–43] and accordingly, the orbital magnetism is significantly different from the conventional Landau diamagnetism.[38,44–56] The orbital susceptibility of bulk graphene diverges when the Fermi energy resides at Dirac point, but vanishes inside the conduction or the valence band. Finite-size effect on this singular diamagnetism has been theoretically studied for carbon nanotubes[57–59] and graphene ribbons.[13,60] In our previous work,[60] particularly, we found that the susceptibility of graphene ribbon behaves in a complicated manner as a function of Fermi energy, reflecting the subband quantization imposed by the spacial confinement.

In this paper, we consider the orbital diamagnetism of lower dimensional systems—graphene flakes as illustrated in Fig. 1. For each case we calculate the orbital magnetic susceptibility and the diamagnetic electric current distribution using the tight-binding model. We find characteristic properties peculiar to each different case, and also general tendencies independent of the configuration. We also predict that the diamagnetism of graphene can be observed using the alignment of graphene flakes dissolved in a solvent under a magnetic field. The paper is organized as follows. In Sec. II, we introduce tight-binding Hamiltonian and the formulas to describe the orbital magnetic effect. We calculate the magnetic susceptibility and the diamagnetic electric current distribution for graphene flakes in Secs. III and IV, respectively. We make a quantitative comparison between the orbital magnetism and the spin magnetism in Sec. V. We argue the magnetic-field alignment effect in Sec. VI and present a brief conclusion in Sec. VII.

II. FORMULATIONS

Graphene is composed of a honeycomb lattice of carbon atoms, where a unit cell contains A and B sublattices. We consider four different atomic configurations of graphene flakes as shown in Fig. 1, which are characterized by hexagonal or trigonal shape and by armchair or zigzag edge termination. For each case, we range the system size from a few nm to a few tens of nm. We describe the motion of graphene electrons using the nearest-neighbor tight-binding model for p_z atomic orbitals. The Hamiltonian is written as

$$H = -\gamma_0 \sum_{\langle n,m \rangle} e^{i2\pi\phi_{nm}} c_n^\dagger c_m, \qquad (1)$$

where $-\gamma_0$ is the transfer integral, c_n and $c_n^\dagger$ are the annihilation and creation operators of an electron at the site n, respectively, and $\langle n,m \rangle$ represents summation over all nearest-neighbor sites. The parameter γ_0 was experimentally estimated in the bulk graphite as $\gamma_0 \approx 3$ eV.[61] The system is under a uniform magnetic field $\boldsymbol{B}$ perpendicular to the graphene plane, which is incorporated by the Peierls phase ϕ_{nm},

$$\phi_{nm} = \frac{e}{ch} \int_n^m d\boldsymbol{\ell} \cdot \boldsymbol{A}, \qquad (2)$$

where $\boldsymbol{A}(\boldsymbol{r})$ is the vector potential giving the magnetic field by $\boldsymbol{B} = \nabla \times \boldsymbol{A}$.

For each single graphene flake, we diagonalize Hamiltonian Eq. (1) and obtain a set of eigenenergies ε_i. The
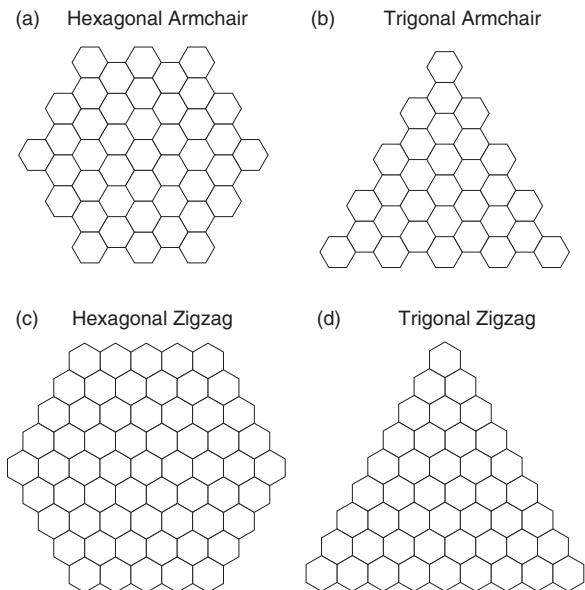
FIG. 1. Atomic structures of (a) hexagonal armchair, (b) trigonal armchair, (c) hexagonal zigzag, and (d) trigonal zigzag graphene flakes.

thermodynamical potential at temperature T and chemical potential μ is written as

$$\Omega = -k_B T \sum_i \ln\{1 + \exp[(\mu - \varepsilon_i)/k_B T]\}. \quad (3)$$

The magnetic susceptibility per unit area is given by

$$\chi = -\frac{1}{S}\left(\frac{\partial^2 \Omega}{\partial B^2}\right)_{\mu,T}\bigg|_{B=0}, \quad (4)$$

where S is the area of the system. To calculate this, we obtain the eigenenergies at zero magnetic field and a small finite magnetic field, and numerically calculate the derivative of the thermodynamic potential.

The electric current from the site m to n is calculated by an operator,

$$J_{nm} = -i\frac{e\gamma_0}{\hbar}(e^{i2\pi\phi_{nm}}c_n^\dagger c_m - \text{H.c.}). \quad (5)$$

We obtain the expectation value of J_{mn} for each bond using the eigenstates at a sufficiently weak magnetic field, where the current amplitude behaves linearly to B.

For the later references, let us review the orbital magnetism of the bulk graphene. The low-energy physics of graphene electrons can be effectively described by the continuum massless Dirac Hamiltonian[37–43] and the orbital susceptibility is calculated for this model as[38,48,53]

$$\chi_{\text{eff}}(\mu; T) = -g_v g_s \frac{e^2 v^2}{24\pi c^2} \frac{1}{k_B T \cosh^2[\mu/(2k_B T)]}, \quad (6)$$

where $g_v = g_s = 2$ are the valley and spin degeneracies, respectively, v is the band velocity related to the transfer integral by $\hbar v = \sqrt{3}a\gamma_0/2$, and $a \approx 0.246$ nm is the lattice constant of graphene. At $T = 0$, Eq. (6) becomes a δ function,

$$\chi_{\text{eff}}(\mu; T = 0) = -g_v g_s \frac{e^2 v^2}{6\pi c^2}\delta(\mu). \quad (7)$$

III. MAGNETIC SUSCEPTIBILITY

Figure 2 shows the susceptibility against the chemical potential for four types of the graphene flakes with several different temperatures. The areas of the flakes are taken to be nearly equal to $S \approx (23.5 \text{ nm})^2$, which includes 1.1×10^4 of hexagonal unit cells. The horizontal and vertical axes are scaled by

$$\varepsilon_0 = \frac{\hbar v}{\sqrt{S}}, \quad (8)$$

$$\chi_0 = \frac{g_v g_s e^2 v^2}{6\pi c^2 \varepsilon_0}, \quad (9)$$

respectively. ε_0 represents the energy scale in the Dirac cone associated with the length scale $\sqrt{S}$. We also calculated the susceptibility for different system sizes and found that for each of four types, the susceptibility and the level structure plotted in this scale becomes almost universal as long as $\sqrt{S} \gg a$. This is naturally expected from the fact that the low-energy physics are well described by the Dirac Hamiltonian.

The upper figure in each panel presents the energy-level structure at $B = 0$, where dashed (black) lines are nondegenerate levels, and solid (red) lines are twofold degenerate levels. In the low-temperature regime, $k_B T \ll \varepsilon_0$, we observe that the susceptibility abruptly changes at every single energy level, and in particular, it exhibits sharp spikes toward the paramagnetic direction (downward in the figure) at twofold degenerate levels. This is because the degenerate states, having opposite magnetic moments, split linearly in magnetic field just like spin Zeeman splitting, and induce paramagnetism in an analogous way to spin Pauli paramagnetism. The contribution to the orbital susceptibility (per area) from the degenerate states at E_0 is written as

$$\chi = \frac{2m^2}{S}\delta(\mu - E_0), \quad (10)$$

where $\pm m$ are the magnetic moments of the doublet. The typical magnitude of m is shown to be $\sqrt{S}ev/c$, which is the only magnetic-moment scale in the massless Dirac system.

The major difference between armchair flakes and zigzag flakes comes from the existence of the zero-energy edge states peculiar to the zigzag edge.[11–13] In the triangular zigzag flake, Fig. 2(d), there are a number of energy levels exactly at zero energy,[19] of which wave functions are shown to be localized at the edge, and the degeneracy is the order of $\sim\sqrt{S}/a$. Remarkably, the susceptibility in the low-temperature regime is completely flat at these levels, meaning that the edge states have absolutely no contribution to the orbital magnetism. This is simply because the edge states are locked to zero energy even in the presence of magnetic field, and never participate in the total-energy change. In the hexagonal zigzag flake, Fig. 2(c), on the other hand, the edge levels slightly shift from zero energy, leading to some small contributions to the orbital susceptibility. The energy shift arises because the edge states on neighboring sides of the hexagon always reside at different sublattices, and they are hybridized by some finite matrix element including γ_0. Nevertheless, the edge states do not play a significant role in the overall behavior of the orbital magnetism.

As the temperature increases, the spikes and steps in the susceptibility are smeared out into an oscillatory curve. The oscillation eventually disappears in $k_B T/\varepsilon_0 \gtrsim 1$, leaving a
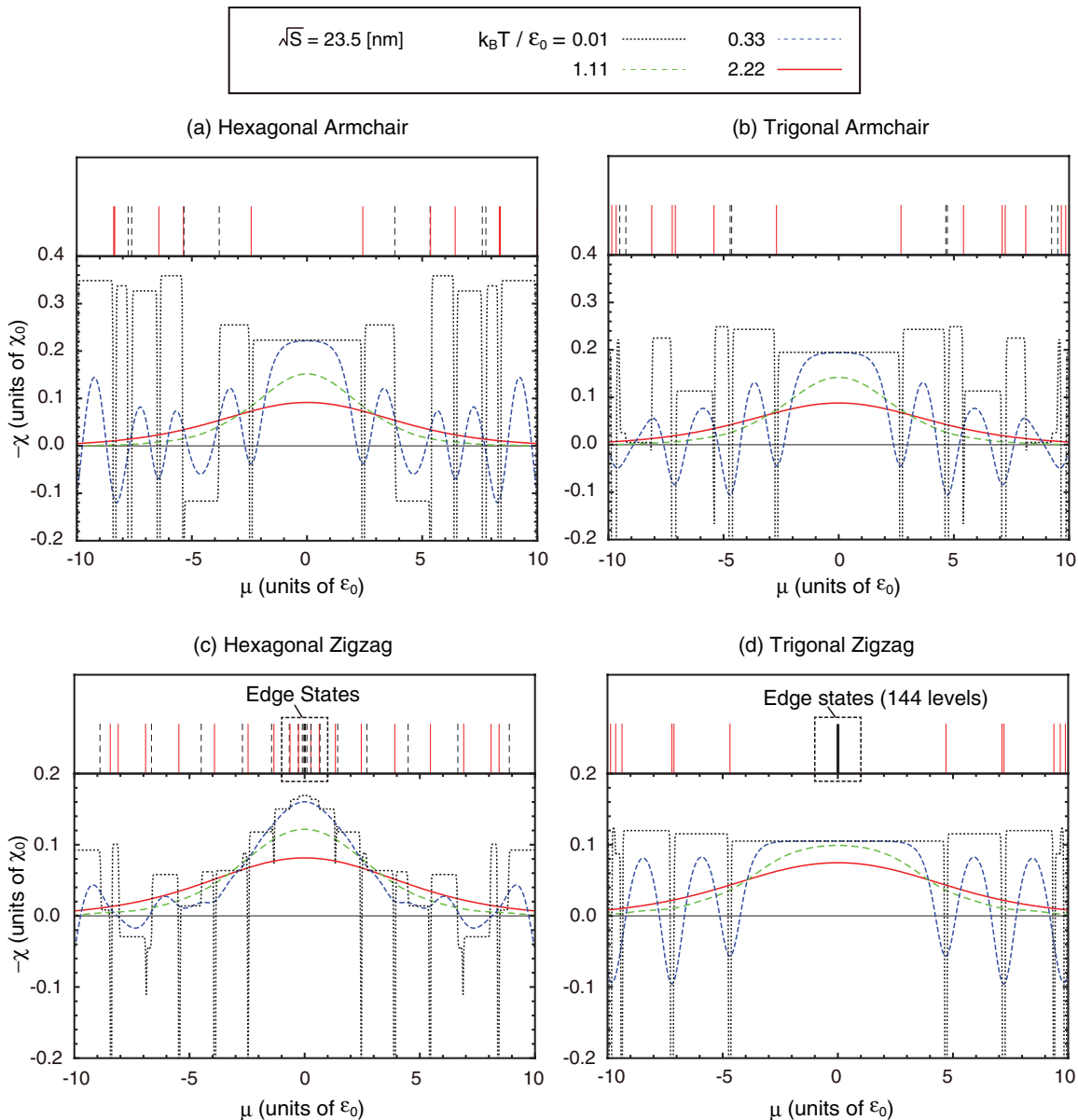
FIG. 2. (Color online) Orbital magnetic susceptibility as a function of μ in (a) hexagonal armchair, (b) trigonal armchair, (c) hexagonal zigzag, and (d) trigonal zigzag graphene flakes with the size of $\sqrt{S} \approx 23.5$ nm. In each figure, the upper panel presents the energy spectrum, where dashed (black) lines represent nondegenerate levels, and solid (red) lines represent twofold degenerate levels.

single diamagnetic peak at the Dirac point, which corresponds to the thermally broadened δ function in the bulk limit, Eq. (6). In Fig. 3, we present an extended plot of the susceptibility curves at $k_B T/\varepsilon_0 = 2.22$ over the whole band region, for different types of graphene flakes with $\sqrt{S} \approx 23.5$ nm. The energy axis is now scaled by absolute unit γ_0. We see that the finite-size effect almost vanishes in this temperature regime, giving a universal curve independent of the atomic configuration. The curves still slightly differ near the central peak, because the level spacing around the Dirac point, which is about $\sim \varepsilon_0$, is not completely negligible compared to $k_B T$ at this particular system size. This small variance would vanish in larger flakes which satisfy $k_B T \gg \varepsilon_0$.

The curve is characterized by the strong diamagnetic peak at the Dirac point and some smaller structures off the Dirac

point. The contribution from the lower-half spectrum adds up to a paramagnetic offset to the central diamagnetic peak.[56] Namely, the susceptibility near $\mu = 0$ is approximately written as

$$\chi(\mu; T) \approx \chi_{\text{eff}}(\mu; T) + \chi_{\text{para}}, \tag{11}$$

where χ_{eff} is given by Eq. (6), and

$$\chi_{\text{para}} \approx 0.37 \times \frac{g_v g_s e^2 v^2}{6\pi c^2 \gamma_0}. \tag{12}$$

The offset χ_{para} is much smaller than the height of the central peak $\approx g_v g_s e^2 v^2/(24\pi c^2 k_B T)$, since $k_B T$ is usually much smaller than γ_0. Outside the Dirac cone region, we see tiny Landau diamagnetism in the quadratic band bottom at
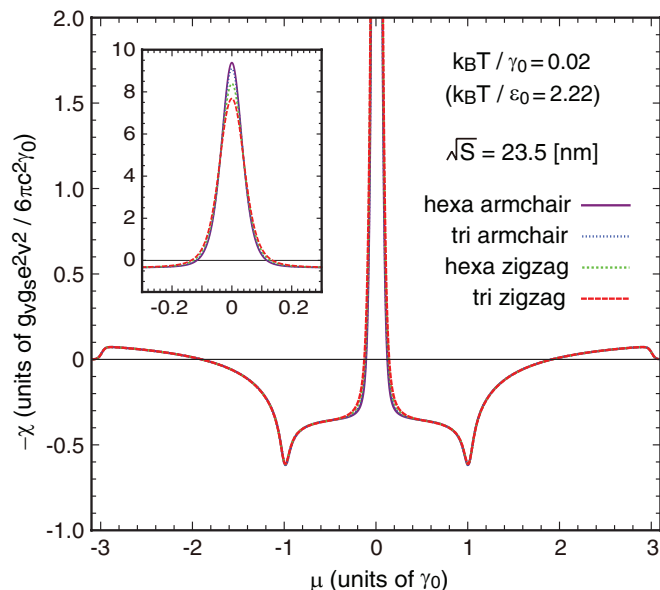
FIG. 3. (Color online) Extended plot of the susceptibility curves in Fig. 2 over the whole band region, for the four types of graphene flakes at $k_B T/\varepsilon_0 = 2.22$. The energy axis is now scaled by absolute unit γ_0, in which the temperature amounts to $k_B T/\gamma_0 = 0.02$. Inset shows the detail of the central peak.

$\mu = \pm 3\gamma_0$, and paramagnetism around the Van Hove singularity at $\mu = \pm \gamma_0$.[53–56]

To analyze the size dependence quantitatively, we plot $\chi(\mu = 0; T)$ of hexagonal armchair flakes with different sizes in Figs. 4(a) and 4(b). Panels (a) and (b) present the same information but in different fashions: (a) shows χ in the absolute units γ_0 and $g_v g_s e^2 v^2/(6\pi c^2 \gamma_0)$ for horizontal and vertical axes, respectively, while (b) shows $\chi - \chi_{\text{para}}$ i.e., the contribution from the Dirac cone, with relative units ε_0 and χ_0 depending on the system size. In (b), we see that the curve converges to a single universal curve as the size increases, indicating that the physics there is well described by effective Dirac equation. The susceptibility approaches the bulk limit χ_{eff} in the high-temperature region $k_B T \gg \varepsilon_0$, whereas in $k_B T \lesssim \varepsilon_0$ it deviates from χ_{eff} and reaches some finite maximum value. When we consider the susceptibility of a single graphene flake, χS, at a fixed absolute temperature, it scales in proportion to $\chi_0 S \propto S^{3/2}$ in the low-temperature regime $k_B T \lesssim \varepsilon_0$, while it is just proportional to S in the high-temperature regime $k_B T \gg \varepsilon_0$ where χ is equal to the bulk limit.

The detail of the universal curve in Fig. 4(b) depends on the flake shape and the edge configuration. In Fig. 4(c), we present plots similar to Fig. 4(b) for four different types of graphene flakes with the same size $\sqrt{S} \approx 23.5$ nm, which is sufficiently large to achieve the universal limit. In low temperatures, the susceptibility tends to be larger in an armchair flake than in a zigzag flake, and larger in a hexagonal flake than in a trigonal flake. In the high-temperature region, on the other hand, all the curves approach the same bulk limit. A similar edge dependence was previously found in graphene ribbons, where armchair ribbons generally exhibit larger diamagnetism than zigzag ribbons.[13,60]
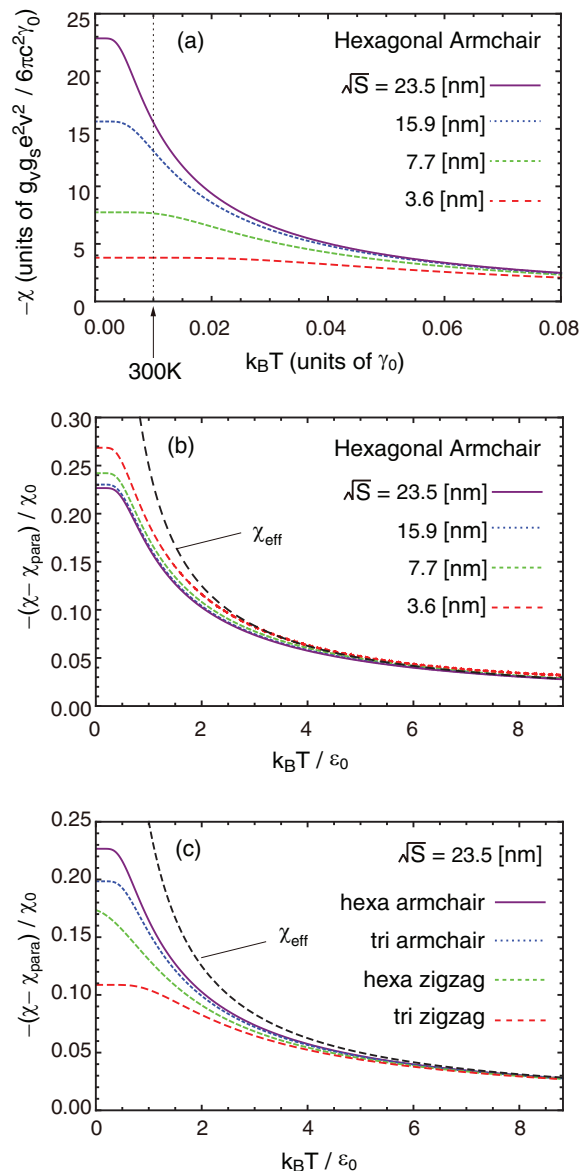

FIG. 4. (Color online) (a) $\chi(\mu = 0; T)$ of hexagonal armchair flakes with several different sizes, plotted in the absolute units γ_0 and $g_v g_s e^2 v^2/(6\pi c^2 \gamma_0)$. (b) $\chi(\mu = 0; T) - \chi_{\text{para}}$ of the same systems, plotted in the relative units ε_0 and χ_0. (c) Plot similar to (b) for different types of graphene flakes with the size $\sqrt{S} \approx$ 23.5 nm.

IV. DIAMAGNETIC CURRENT DISTRIBUTION

Figure 5 shows the diamagnetic current distribution induced by the magnetic field in the four types of graphene flakes of the size $\sqrt{S} \approx 23.5$ nm at several different temperatures. To visualize the global current circulation, we illustrate continuous flux lines obtained by smoothing the original discrete current J_{mn} on each bond, which is shown in the left inset. Specifically, we find a certain potential function Ψ which satisfies $\boldsymbol{J} = \boldsymbol{e}_z \times \nabla \Psi$, and obtain the equipotential lines of Ψ as the current flux lines. At zero temperature, the flux circulates entirely on the system reflecting the absence of the characteristic wavelength in graphene. As temperature becomes higher, it is going to be localized near the edge.
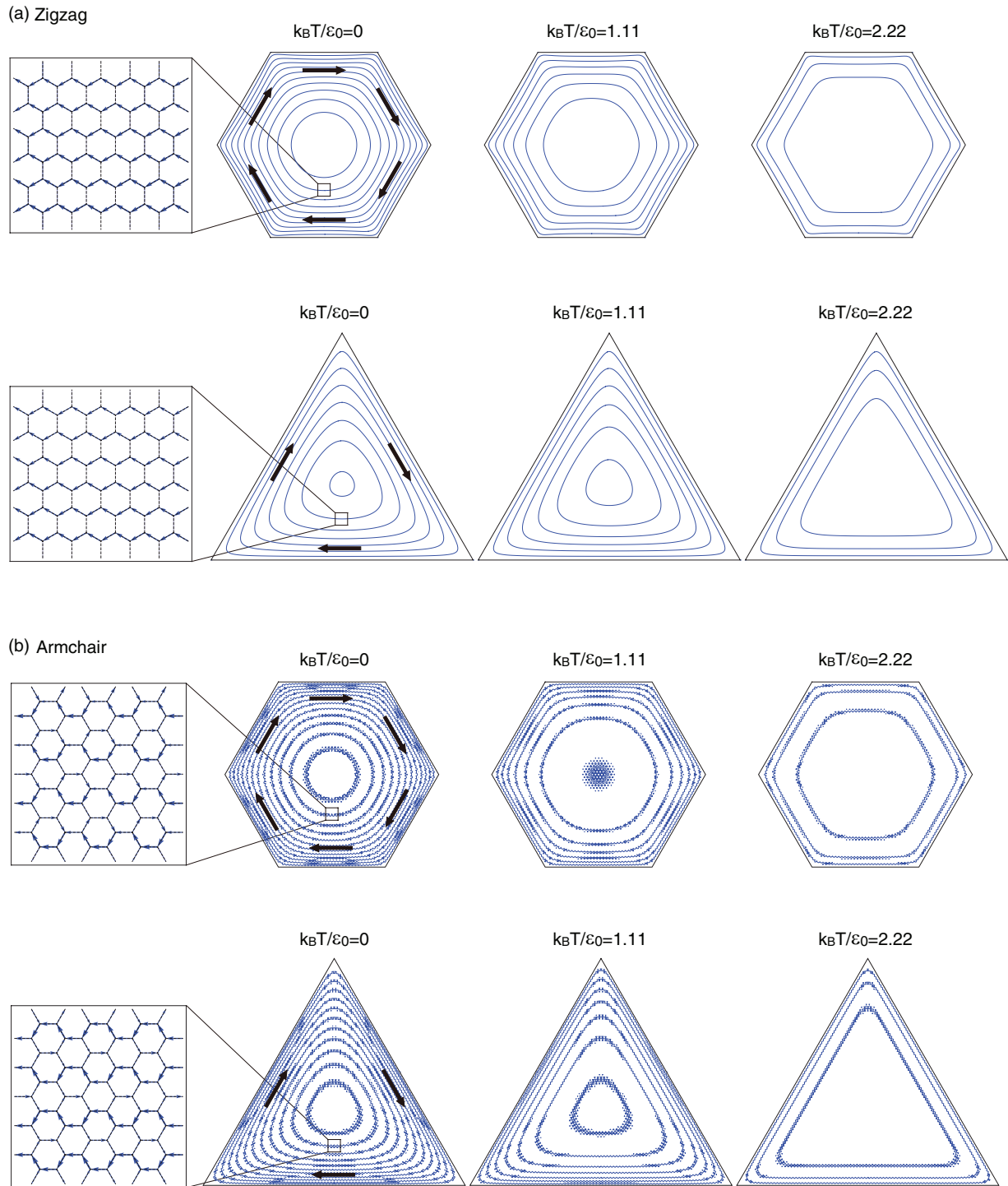
FIG. 5. (Color online) Diamagnetic current distribution in different types of graphene flakes of the same size $\sqrt{S} \approx 23.5$ nm at several different temperatures. Continuous flux lines are obtained by smoothing the original discrete current on each bond, which is shown in the left.

The current circulation of zigzag and armchair graphene flakes are globally similar, but the flux lines of armchair flakes exhibit some roughness while it is not observed in zigzag flakes. This actually corresponds to the atomic-scale current circulation in the Kekulé pattern seen in the original current map (left inset),[13] which is caused by the intervalley (between K and K') hybridization peculiar to the armchair edge.

Figure 6 shows the detailed plots of the electric current as a function of position from the boundary to the center, calculated for (a) the zigzag and (b) armchair flakes. The position is labeled by the bond index defined in the inset, and

(a) Zigzag
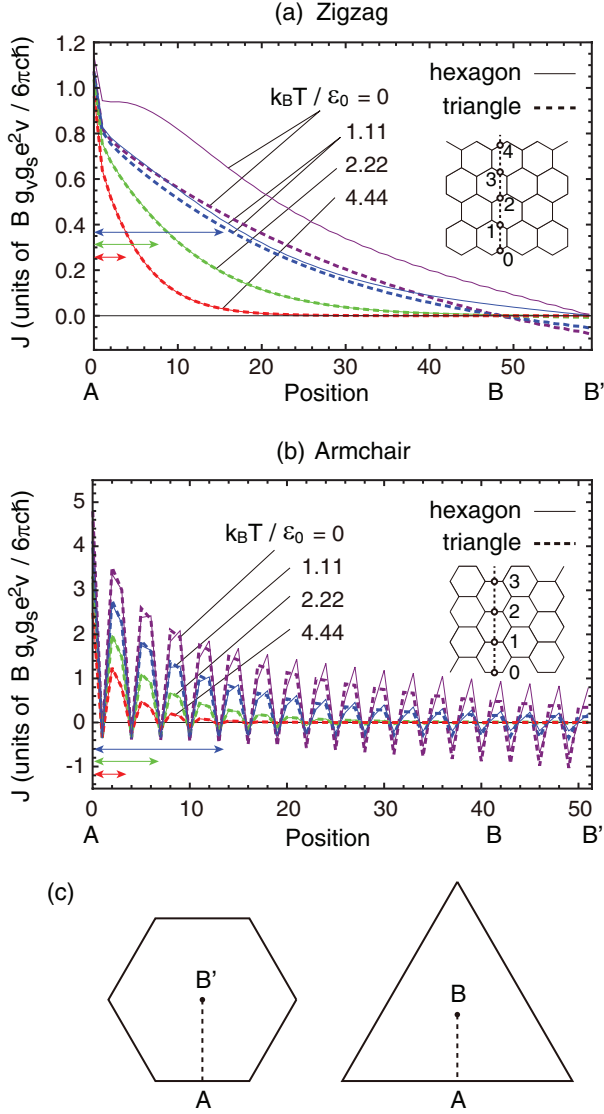

(b) Armchair

(c)

FIG. 6. (Color online) Electric current as a function of position from the boundary to the center, in (a) the zigzag and (b) armchair flake with $\sqrt{S} \approx 23.5$ nm. The position is labeled by the bond index defined in the inset, and A and B (B') represent the border and the center of triangle (hexagon), respectively, which are specified in (c). Horizontal arrows indicate λ_{edge} for $k_B T / \varepsilon_0 = 1.11$, 2.22, and 4.44.

A and B (B') correspond to the edge and the center of triangle (hexagon), respectively, which are depicted in Fig. 6(c). The current distribution is more localized to the edge when T becomes higher, and the typical depth of the edge current is characterized by

$$\lambda_{\text{edge}} = \frac{\hbar v}{2\pi k_B T}, \tag{13}$$

in accordance with the result for graphene ribbons.[60] The current distribution in the atomic scale strongly depends on the edge type. We can show that, however, the integrated edge current approximates $c\chi_{\text{eff}}B$ independently of the edge type, in the high-temperature regime $k_B T / \varepsilon_0 \gtrsim 2$. This is consistent with the fact that the orbital susceptibility

is then given by the bulk limit regardless of the atomic configuration. When comparing hexagonal and triangular flakes of the same edge type, we see that the curves are almost completely equivalent in $k_B T / \varepsilon_0 \gtrsim 2$. This suggests that the edge current distribution in high temperature is solely determined by the local edge configuration, independently of the global shape.

V. COMPARISON TO SPIN PARAMAGNETISM

The orbital magnetism always competes with the spin paramagnetism which has been neglected so far. When we include spin Zeeman splitting, each spinless energy level at E_0 acquires the Pauli paramagnetism

$$\chi_{\text{Pauli}} = \frac{1}{S}\left(\frac{g}{2}\mu_B\right)^2 2\delta(\mu - E_0), \tag{14}$$

where $g \sim 2$ is the g factor for a graphene electron, $\mu_B = e\hbar/(2m_0 c)$ is the Bohr magneton, and m_0 is the bare electron mass. This is similar to the orbital contribution of Eq. (10) for doubly degenerate levels, while the orbital magnetic moment m there is now replaced with $g\mu_B/2$. In the flakes of $S > (1 \text{ nm})^2$, μ_B is much smaller than the typical magnitude of m, which is $\approx \sqrt{S}ev/c$, suggesting that the Pauli paramagnetic effect is typically much smaller than the orbital effect. This is in contrast to conventional electron systems where orbital magnetic moment and spin magnetic moment are both of the order of μ_B.[62]

In a zigzag graphene flake, the highly degenerate edge states at zero energy give exceptionally large Pauli paramagnetism. The contribution is written as

$$\chi_{\text{Pauli}} = \frac{N_{\text{edge}}}{S}\left(\frac{g}{2}\mu_B\right)^2 2\delta(\mu), \tag{15}$$

where $N_{\text{edge}}(\sim \sqrt{S}/a)$ is the number of edge states per spin. In the low-temperature regime such that $k_B T \ll \varepsilon_0$, this is dominant over the orbital effect near zero energy, since the orbital susceptibility does not diverge at edge states as already shown. In the high-temperature regime $k_B T \gg \varepsilon_0$, the δ function is thermally broadened and it should be compared to the bulk orbital susceptibility χ_{eff}, Eq. (6). The ratio between two opposite components approximates[60]

$$\left|\frac{\chi_{\text{Pauli}}}{\chi_{\text{eff}}}\right| \sim \frac{3\pi}{g_v g_s}\left(\frac{g}{2}\frac{\hbar}{m_0 va}\right)^2 \frac{a}{\sqrt{S}} \sim 0.4 \times \frac{a}{\sqrt{S}}, \tag{16}$$

so that the Pauli paramagnetism is negligible in a large flake with $\sqrt{S} \gg a$. It should be noted that graphene flakes may have lattice vacancies and/or adatoms depending on the experimental condition, and the impurity levels given by these defects contribute to additional Pauli paramagnetism.

We remark that several experimental studies reported the evidence of ferromagnetic spin ordering in graphene-based materials.[28–30,32] The origin of the spontaneous spin magnetism is still under debate, while it is supposed to be caused by the electron-electron interaction (neglected in this work) with the atomic defects, or highly degenerate edge states in zigzag edges.[13,33,34,63,64] Besides the spin magnetism, the orbital magnetism itself may also be changed by the electron-electron interaction through the modification of the

energy band. In triangular zigzag graphene flakes, in particular, it is predicted that the electron-electron interaction may open an energy gap in the edge-state levels.[33,34] Considering that the edge states do not contribute much to the orbital magnetism, this would give some minor effects on the orbital susceptibility near zero energy.

VI. MAGNETIC FIELD ALIGNMENT OF GRAPHENE FLAKES

The diamagnetism of graphene can be possibly observed using the magnetic-field alignment of graphene nanoflakes dissolved in a solvent, similarly to the experiments for the carbon nanotube.[65,66] In a magnetic field, the graphene flakes tend to be oriented parallel to the field direction, because the field component penetrating the graphene plane raises the total energy due to the diamagnetism. If we assume that the graphene flakes are planer and rigid, the condition to achieve the alignment is roughly estimated as

$$\frac{1}{2}\chi B^2 S \gtrsim k_B T. \tag{17}$$

For the graphene flakes $\sqrt{S} \approx 23.5$ nm at $T = 300$ K, for example, the required field becomes $B \gtrsim 9$ T.

We calculate the angle distribution of graphene flakes with various sizes using the Maxwell-Boltzmann statistics. In the thermal equilibrium, the probability that the normal of the graphene plane is inclined from the magnetic field by θ to $\theta + d\theta$ is written as $P(\cos\theta)d(\cos\theta)$, where

$$P(\cos\theta) = \frac{\exp[-\beta U(\cos\theta)]}{\int_{-1}^{1} \exp[-\beta U(\cos\theta)]d(\cos\theta)}, \tag{18}$$

with $U(\cos\theta) = -(1/2)\chi S B^2 \cos^2\theta$ and $\beta = 1/(k_B T)$. Figure 7 plots the distribution function $P(\cos\theta)$ calculated for hexagonal armchair flakes with several sizes at $T = 300$ K, using χ in Fig. 4(a). We see that the alignment occurs more strongly in larger flakes, because the magnetization of a single flake, χSB, is greater for larger S. Note that it is not only due to a linear factor S, but also because χ increases in larger S as shown in Fig. 4(a).

VII. CONCLUSION

We have studied the orbital diamagnetism of the graphene flakes with various shapes and edge configurations using the tight-binding approximation. We found that the behavior is significantly different depending on the relative magnitude of the thermal broadening energy $k_B T$ to the typical energy-level spacing $\varepsilon_0 = \hbar v/\sqrt{S}$. In the low-temperature regime where $k_B T \ll \varepsilon_0$, the susceptibility as a function of Fermi energy rapidly changes between diamagnetism and paramagnetism in accordance with the level structure depending on the specific atomic structure of the flake. The susceptibility at the zero Fermi energy is found to be generally larger in armchair flakes than in zigzag flakes, and larger in hexagonal flakes than in trigonal flakes. In the high-temperature regime $k_B T \gtrsim 2\varepsilon_0$, on the other hand, the discrete structures due to the finite-size effect are all gone, and the susceptibility approximates the bulk limit independently of the shape and the edge configuration of the flake. Considering ε_0 is written as 8000 K/$\sqrt{S}$ nm using the graphene's band velocity, we find that the room temperature
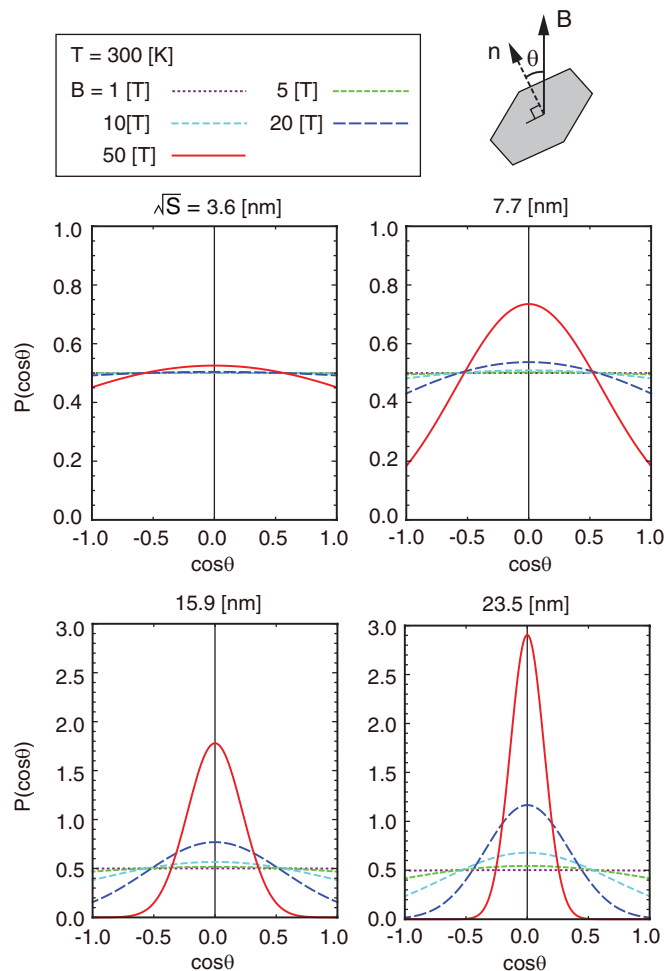

FIG. 7. (Color online) Angle distribution of hexagonal armchair flakes in magnetic fields at $T = 300$ K.

belongs to the low-temperature regime for a flake of a few nm, while it is in the high-temperature regime for a flake more than 50 nm.

In the low-temperature regime, the diamagnetic current circulates entirely on the graphene flakes, reflecting the absence of characteristic length scale. As the temperature increases, the current gradually becomes to circulate only near the edge, with the characteristic depth of $\lambda_{edge} = \hbar v/2\pi k_B T$. The local current distribution along the cross section perpendicular to the boundary is insensitive to the global shape of the flake, but significantly different between armchair and zigzag edges.

We predict that the diamagnetism of graphene can be possibly observed using the magnetic-field alignment of graphene flakes. We estimated the angle distribution at various magnetic fields, and found that a strong alignment can be realized in the feasible magnetic field range for flakes of $S \gtrsim (10 \text{ nm})^2$.

[1] M. Y. Han, B. Özyilmaz, Y. Zhang, and P. Kim, Phys. Rev. Lett. **98**, 206805 (2007).

[2] Z. Chen, Y.-M. Lin, M. J. Rooks, and P. Avouris, Physica E **40**, 228 (2007).

[3] X. Li, X. Wang, L. Zhang, S. Lee, and H. Dai, Science **319**, 1229 (2008).

[4] D. V. Kosynkin, A. L. Higginbotham, A. Sinitskii, J. R. Lomeda, A. Dimiev, B. K. Price, and J. M. Tour, Nature (London) **458**, 872 (2009).

[5] L. Y. Jiao, L. Zhang, X. R. Wang, G. Diankov, and H. J. Dai, Nature (London) **458**, 877 (2009).

[6] Y. Kobayashi, K. I. Fukui, T. Enoki, K. Kusakabe, and Y. Kaburagi, Phys. Rev. B **71**, 193406 (2005).

[7] T. Enoki, Y. Kobayashi, and K. Fukui, Inter. Rev. Phys. Chem. **26**, 609 (2007).

[8] D. Geng, B. Wu, Y. Guo, L. Huand, Y. Xue, J. Chen, G. Yu, L. Jiang, W. Hu, and Y. Liu, Proc. Natl. Acad. Sci. USA **109**, 7992 (2012).

[9] S. K. Hamalainen, Zh. Sun, M. P. Boneschanscher, A. Uppstu, M. Ijas, A. Harju, D. Vanmaekelbergh, and P. Liljeroth, Phys. Rev. Lett. **107**, 236803 (2011).

[10] D. Subramaniam, F. Libisch, Y. Li, C. Pauly, V. Geringer, R. Reiter, T. Mashoff, M. Liebmann, J. Burgdorfer, C. Busse, T. Michely, R. Mazzarello, M. Pratzer, and M. Morgenstern, Phys. Rev. Lett. **108**, 046801 (2012).

[11] M. Fujita, K. Wakabayashi, K. Nakada, and K. Kusakabe, J. Phys. Soc. Jpn. **65**, 1920 (1996).

[12] K. Nakada, M. Fujita, G. Dresselhaus, and M. S. Dresselhaus, Phys. Rev. B **54**, 17954 (1996).

[13] K. Wakabayashi, M. Fujita, H. Ajiki, and M. Sigrist, Phys. Rev. B **59**, 8271 (1999).

[14] M. Ezawa, Phys. Rev. B **73**, 045432 (2006).

[15] L. Brey and H. A. Fertig, Phys. Rev. B **73**, 195408 (2006).

[16] L. Brey and H. A. Fertig, Phys. Rev. B **73**, 235411 (2006).

[17] Y-W. Son, M. L. Cohen, and S. G. Louie, Phys. Rev. Lett. **97**, 216803 (2006).

[18] Y-W. Son, M. L. Cohen, and S. G. Louie, Nature (London) **444**, 347 (2006).

[19] M. Ezawa, Phys. Rev. B **76**, 245415 (2007).

[20] M. Ezawa, Phys. Rev. B **81**, 201402 (2010).

[21] M. Zarenia, A. Chaves, G. A. Farias, and F. M. Peeters, Phys. Rev. B **84**, 245403 (2011).

[22] P. Potasz, A. D. Guclu, and P. Hawrylak, Phys. Rev. B **81**, 033403 (2010).

[23] D. A. Bahamon, A. L. C. Pereira, and P. A. Schulz, Phys. Rev. B **79**, 125414 (2009).

[24] J. Akola, H. P. Heiskanen, and M. Manninen, Phys. Rev. B **77**, 193410 (2008).

[25] Z. Z. Zhang, K. Chang, and F. M. Peeters, Phys. Rev. B **77**, 235411 (2008).

[26] D. P. Kosimov, A. A. Dzhurakhalov, and F. M. Peeters, Phys. Rev. B **81**, 195414 (2010).

[27] K. S. Krishnan and N. Ganguli, Nature (London) **139**, 155 (1937); Z. Krist. A **100**, 530 (1939).

[28] P. Esquinazi, A. Setzer, R. Hohne, C. Semmelhack, Y. Kopelevich, D. Spemann, T. Butz, B. Kohlstrunk, and M. Losche, Phys. Rev. B **66**, 024429 (2002).

[29] P. Esquinazi, D. Spemann, R. Hohne, A. Setzer, K.-H. Han, and T. Butz, Phys. Rev. Lett. **91**, 227201 (2003).

[30] T. Enoki and K. Takai, Solid State Commun. **149**, 1144 (2009).

[31] M. Sepioni, R. R. Nair, S. Rablen, J. Narayanan, F. Tuna, R. Winpenny, A. K. Geim, and I. V. Grigorieva, Phys. Rev. Lett. **105**, 207205 (2010).

[32] Y. Wang, Y. Huang, Y. Song, X. Zhang, Y. Ma, J. Liang, and Y. Chen, Nano Lett. **9**, 220 (2009).

[33] J. Fernandez-Rossier and J. J. Palacios, Phys. Rev. Lett. **99**, 177204 (2007).

[34] W. L. Wang, S. Meng, and E. Kaxiras, Nano Lett. **8**, 241 (2008).

[35] K. S. Novoselov, A. K. Geim, S. V. Morozov, D. Jiang, M. I. Katsnelson, I. V. Grigorieva, S. V. Dubonos, and A. A. Firsov, Nature (London) **438**, 197 (2005).

[36] Y. Zhang, Y.-W. Tan, H. L. Stormer, and P. Kim, Nature (London) **438**, 201 (2005).

[37] P. R. Wallace, Phys. Rev. **71**, 622 (1947).

[38] J. W. McClure, Phys. Rev. **104**, 666 (1956).

[39] J. C. Slonczewski and P. R. Weiss, Phys. Rev. **109**, 272 (1958).

[40] D. P. DiVincenzo and E. J. Mele, Phys. Rev. B **29**, 1685 (1984).

[41] G. W. Semenoff, Phys. Rev. Lett. **53**, 2449 (1984).

[42] N. H. Shon and T. Ando, J. Phys. Soc. Jpn. **67**, 2421 (1998).

[43] T. Ando, J. Phys. Soc. Jpn. **74**, 777 (2005), and references cited therein.

[44] J. W. McClure, Phys. Rev. **119**, 606 (1960).

[45] S. G. Sharapov, V. P. Gusynin, and H. Beck, Phys. Rev. B **69**, 075104 (2004).

[46] H. Fukuyama, J. Phys. Soc. Jpn. **76**, 043711 (2007).

[47] M. Nakamura, Phys. Rev. B **76**, 113301 (2007).

[48] M. Koshino and T. Ando, Phys. Rev. B **75**, 235333 (2007).

[49] A. Ghosal, P. Goswami, and S. Chakravarty, Phys. Rev. B **75**, 115123 (2007).

[50] T. Ando, Physica E **40**, 213 (2007).

[51] M. Koshino, Y. Arimura, and T. Ando, Phys. Rev. Lett. **102**, 177203 (2009).

[52] M. Koshino and T. Ando, Phys. Rev. B **81**, 195431 (2010).

[53] S. A. Safran and F. J. DiSalvo, Phys. Rev. B **20**, 4889 (1979).

[54] J. Blinowski and C. Rigaux, J. Phys. (Paris) **45**, 545 (1984).

[55] R. Saito and H. Kamimura, Phys. Rev. B **33**, 7218 (1986).

[56] G. Gomez-Santos and T. Stauber, Phys. Rev. Lett. **106**, 045504 (2011).

[57] H. Ajiki and T. Ando, J. Phys. Soc. Jpn. **62**, 2470 (1993); **63**, 4267 (1994) (Erratum).

[58] H. Ajiki and T. Ando, J. Phys. Soc. Jpn. **64**, 4382 (1995).

[59] M. Yamamoto, M. Koshino, and T. Ando, J. Phys. Soc. Jpn. **77**, 084705 (2008).

[60] Y. Ominato and M. Koshino, Phys. Rev. B **85**, 165454 (2012).

[61] M. S. Dresselhaus and G. Dresselhaus, Adv. Phys. **51**, 1 (2002).

[62] R. Kubo and Y. Obata, J. Phys. Soc. Jpn. **11**, 547 (1956).

[63] M. Grujic, M. Tadic, and F. M. Peeters, Phys. Rev. B **87**, 085434 (2013).

[64] K. Szalowski, Phys. Rev. B **84**, 205409 (2011).

[65] D. A. Walters, M. J. Casavant, X. C. Qin, C. B. Huffman, P. J. Boul, L. M. Ericson, E. H. Haroz, M. J. O'Connell, K. Smith, D. T. Colbert, and R. E. Smalley, Chem. Phys. Lett. **338**, 14 (2001).

[66] S. Zaric, G. N. Ostojic, J. Kono, J. Shaver, V. C. Moore, M. S. Strano, R. H. Hauge, R. E. Smalley, and X. Wei, Science **304**, 1129 (2004).